Positron interactions with water–total elastic, total inelastic, and elastic differential cross section measurements

Wade Tattersall,[1,2] Luca Chiari,[3] J. R. Machacek,[1] Emma Anderson,[1] Ron D. White,[2] M. J. Brunger,[3,4] Stephen J. Buckman,[1,4] Gustavo Garcia,[5] Francisco Blanco,[6] and James P. Sullivan[1]

[1]*Centre for Antimatter-Matter Studies, Research School of Physics and Engineering, The Australian National University, Canberra, ACT 0200, Australia*
[2]*Centre for Antimatter-Matter Studies, School of Engineering and Physical Sciences, James Cook University, Townsville, 4810 Queensland, Australia*
[3]*Centre for Antimatter-Matter Studies, School of Chemical and Physical Sciences, Flinders University, GPO Box 2100, Adelaide 5001, South Australia, Australia*
[4]*Institute of Mathematical Sciences, University of Malaya, 50603 Kuala Lumpur, Malaysia*
[5]*Instituto de Fısica Fundamental, Consejo Superior de Investigationes Cientıficas (CSIC), Serrano 113-bis, E-28006 Madrid, Spain*
[6]*Departamento de Fısica Atomica, Molecular y Nuclear, Universidad Complutense de Madrid, E-28040 Madrid, Spain*

Utilising a high-resolution, trap-based positron beam, we have measured both elastic and inelastic scattering of positrons from water vapour. The measurements comprise differential elastic, total elastic, and total inelastic (not including positronium formation) absolute cross sections. The energy range investigated is from 1 eV to 60 eV. Comparison with theory is made with both R-Matrix and distorted wave calculations, and with our own application of the Independent Atom Model for positron interactions. © *2014 AIP Publishing LLC*. [http://dx.doi.org/10.1063/1.4862685]

I. INTRODUCTION

The study of positron interactions with atoms and molecules has entered a new phase of discovery in recent years with the advent of high-flux, high-resolution beams that can be tuned in energy from sub 1 eV to many hundreds of electron volts. These tunable energy beams have been used for a variety of new and accurate studies including low energy annihilation [e.g., Refs. 1 and 2], total scattering,[3] inelastic scattering,[4] positronium (Ps) formation,[5] differential (in angle) measurements,[6] and positronium spectroscopy,[7] to name just a few. This acceleration of experimental activity has been matched by developments with positron scattering theory, with new models for annihilation[8] and scattering[9] being applied in recent years, along with developments in positron transport and modelling.[10, 11]

One of the key drivers for this increase in interest in positron interactions is their use in several medical technologies, both for imaging and therapy. In particular, positron interactions and annihilation lie at the heart of one of the most common cancer diagnostics, positron emission tomography, or PET.[12] In a PET scan a positron-emitting isotope, usually ^{18}F, is introduced to the body, typically latched to glucose to form the radiopharmaceutical FDG, which provides metabolic specificity. The mean emission energy of the positrons is typically several hundreds of keV and they must then thermalize in human tissue, reaching energies below a few hundred eV or less, before they can form positronium (Ps) through an interaction with a molecule in the body, or annihilate directly with a free electron. The annihilation process predominantly produces two back-to-back gamma rays, each

with ∼511 keV in energy, which are detected in coincidence, and imaging software is then used to pinpoint the emission site and, possibly, the site of a tumour.

The thermalisation process, which can involve an energy loss of six orders of magnitude or more, takes place through scattering – ionization, electronic excitation, etc. – and can take considerable time and distance, depending on the medium. As a result, the point of emission of the gamma rays can often be significantly different from the source of positrons (e.g., the tumour site). Thus an understanding of the positron thermalisation process may well contribute to optimizing the technologies and ultimately, informing the development of new positron dosimetry models which are based on quantitative data.

Because of its dominant presence in the body, water (H_2O) is often used as a surrogate in the modelling of the interaction of ionizing radiation with human tissue. In order to accurately model positron transport in water, a number of key elements are required. These include an accurate microscopic picture of the interaction, involving a full and accurate set of scattering cross-sections for positrons in water, and an accurate method of simulating the transport (e.g., a Boltzmann equation analysis or Monte Carlo approach), which uses the microscopic information to provide information on a macroscopic scale.

The first of these two key elements is the focus of the present study – the provision of accurate scattering data for positron interactions with water. The current work follows from our earlier studies of positron interactions in water, where we provided data for the total scattering cross section and for the Ps formation cross section.[13] In this study we add

to that body of data with measurements of total elastic, total inelastic, and elastic differential scattering cross sections (DCS). Here the total inelastic scattering channel includes all processes that involve significant energy loss, other than Ps formation – that is electronic excitation and ionization. This cross section is important in models of positron transport as it provides a means of tracking the energy deposition of the positrons into the medium and also the production of secondary electrons. The differential information is also important as it enables the model to accurately predict the spread of the positrons in the medium. In previous models, these angular effects have either been ignored (isotropic scattering assumed), or based on theoretical data, while for the energy-loss interactions, the usual practice has been to assume they were the same as for electrons. Thus the present work has the potential to significantly improve the quality of the input data to Boltzmann and Monte Carlo models of positron transport in water.[10,11]

Another important issue involving the passage of ionizing radiation through the body, which is of relevance to modeling imaging and therapeutic technologies, is that the primary ionizing radiation liberates copious numbers of low-energy secondary electrons along its path.[14] Typically those electrons are produced with energy less than 20 eV. These low-energy electrons thermalize in human tissue through a variety of energy deposition processes. Although low in energy, they have recently been shown to be a significant source of DNA damage,[15,16] even at energies approaching zero, and hence understanding the transport of low-energy secondary electrons is key to understanding radiation damage and informing dosimetry models. Thus it is important to stress that models of positron transport in human tissue or tissue analogues, must also track the fate of the large numbers of secondary electrons that are produced in the thermalisation of the positron and, as such, an accurate, quantitative set of *both* electron and positron cross sections, for as many scattering processes as is possible, is highly desirable. That is one of the key overall goals of this work, and more broadly, our combined experiment/modeling program.

There are only a few theoretical calculations for positron interactions with water and, where possible, we compare with them in this work. We have also calculated cross sections using the independent atom model (IAM) approach pioneered by Garcia and colleagues (see later). This application involves the calculation of the scattering by the individual H and O atoms, which is then combined using the screening-corrected additivity rule (SCAR), to account for the molecular structure. Results using this IAM-SCAR model, which for simplicity we will refer to simply as the IAM, are presented for the total elastic and total inelastic cross sections (ICS) and differential elastic cross sections.

In Sec. II we briefly discuss the experimental techniques that have been applied in this work. This is followed in Sec. III with a very brief discussion of the present IAM method as applied for positrons in water, and then in Sec. IV we present and discuss our experimental results, including comparisons with theory where possible. We finish with some concluding remarks in the final section of the paper.

II. EXPERIMENTAL APPARATUS AND TECHNIQUES

The experimental apparatus and techniques used for this work have been described in detail previously in a number of papers on both room temperature gas-phase [e.g., Refs. 17 and 18] targets, and targets that are both liquid and gaseous at STP,[13] so we will refrain from a detailed description here. Briefly, positrons, which arise from the radioactive decay of ^{22}Na contained within a sealed source (current activity $\sim$ 30 mCi), are moderated by a solid neon moderator operated at $\sim$7 K and loaded into a Surko buffer gas trap. The trap is operated such that a pulsed positron beam with an energy width of $\sim$60 meV and a repetition rate of $\sim$100 Hz is obtained, with up to 1000 positrons per pulse under optimum conditions. These positrons are then passed through a scattering cell, 100 mm in length, which is connected via gas lines to a sample of water. The trap and gas cell are immersed in an axial magnetic (**B**) field of 0.053 tesla. The target gas pressure in the cell is monitored with a capacitance manometer (MKS Baratron Model: 690A01TRA). The gas cell, gas lines, and gas sample are all held at a temperature of 23 °C and the gas number density is determined with an estimated uncertainty of 2%. Positrons, both scattered and unscattered, that pass through the gas cell are energy analysed with a retarding potential analyser (RPA) and detected with a channel plate electron multiplier. The RPA enables the determination of the parallel energy loss spectrum of the positrons. In addition, the **B** field in the RPA region could be adjusted independently, enabling the contribution from elastic and inelastic channels to be separated, as has also been discussed in detail previously.[19,4] A typical retarding potential energy-loss curve is shown in Figure 1 for an incident energy of 45 eV. The vertical lines indicate the threshold of the first electronic excited
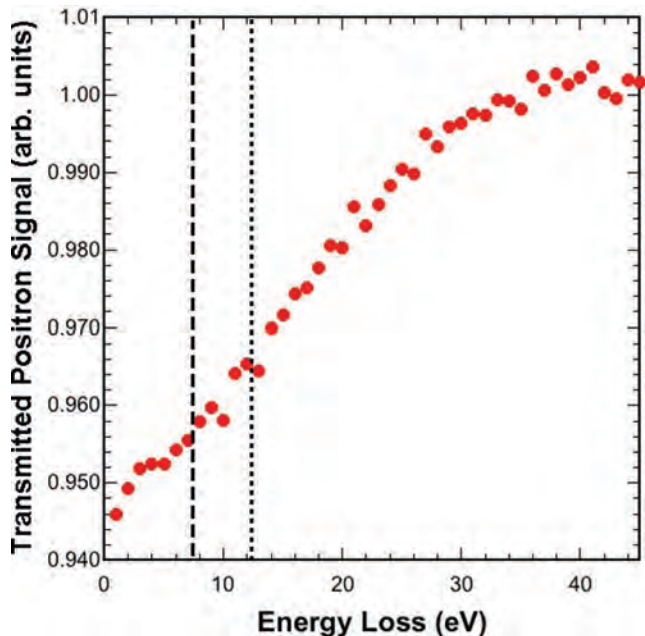
FIG. 1. A typical retarding potential energy-loss, or cut off curve, for 45 eV positrons scattering from H_2O. The vertical lines indicate the first ionization threshold (short dashed) and the threshold for the first accessible electronically excited state, the A^1B_1 state (long dashed).

state, which is accessible by positrons, the $^1B_1$ level, and the first ionization threshold.

The techniques used to obtain the differential elastic scattering cross section have also been discussed in detail previously and we will not repeat that detail here, but refer the reader to those previous discussions, e.g., Refs. 6 and 19.

An important issue for scattering-cell based measurements on all atomic and molecular systems, but particularly those with strong dipole-driven scattering, such as water, is the consideration of forward elastic scattering. We have discussed this issue at some length in several previous papers,[20,6] and will not repeat the detailed rationale here. Suffice it to say that failure to completely account for forward scattering leads to a reduction in the "measured" scattering cross section over the "true" value and, where forward scattering is dominant as in the case of highly polar systems like water, these effects can be significant. In the present experimental arrangement, the angular range ($\pm\theta_c$) in the forward direction over which scattering cannot be accounted for is related to the energy resolution and is energy dependent, being quite large at low energies, but less significant at higher energies, as the angular discrimination of the apparatus is higher (see Table I). If we have knowledge of the differential cross section, for example, from theory, we can estimate the extent that this angular discrimination effect has on the total elastic cross section and correct for it.

III. THEORETICAL CALCULATIONS

Details of the application of the IAM-SCAR[21] method to positron interactions have been provided in a number of previous papers, e.g., Refs. 22 and 23, so we will only very briefly summarise the approach here.

The local complex potential is given by

$$V(r) = V_S(r) + V_P(r) + iV_A(r). \qquad (1)$$

The real part of Eq. (1) drives the elastic scattering dynamics and embraces the electrostatic ($V_S(r)$) and polarization ($V_P(r)$) interactions. The imaginary part ($V_A(r)$) describes all the inelastic processes that are considered as absorption of flux from the incident positron beam. The static potential was obtained from the charge density derived from Hartree–Fock atomic wavefunctions. The dipole plus quadrupole polarization potential was developed from that reported by McEachran *et al.*[24] for Ne, but scaled by a constant in order to match the known dipole and quadrupole polarizabilities of the H and O atoms. The absorption potential accounts for the electronic excitations, positronium (Ps) formation, and direct

TABLE I. Estimated missing angular range (θ_c) for a range of energies within the present study.

Energy (eV)	θ_c
5	23
6	21
10	16
20	11
30	9

ionization. However, owing to the challenging nature of representing the Ps formation channel, the definition of the threshold energy for the absorption potential can be critical. Here we adopt a phenomenological approach where the absorption threshold adopts the form of an energy-dependent parameter:

$$\Delta(E) = \Delta - (\Delta - \Delta_P)exp(-(E - \Delta_P)/E_m), \qquad (2)$$

where Δ is the lowest excitation energy of the atom, Δ_P is the Ps formation threshold energy, and E_m is a characteristic energy at which the inelastic ICS, without Ps formation, reaches its maximum (here $E_m = 30$ eV). From Eq. (2) it is clear that $\Delta(E) \approx \Delta_P$ for energies around the Ps formation energy and $\Delta(E) \approx \Delta$ at higher energies. Note that using both threshold parameters, $\Delta(E)$ and Δ, alternatively, positronium formation cross sections can be derived from the difference between the corresponding inelastic cross sections.

To calculate the cross sections for positron collisions with H_2O, the additivity rule (AR) is then applied to the optical model results for each constituent atom. In this approach, the molecular scattering amplitude stems from the sum of all the relevant atomic amplitudes, including the phase coefficients, which gives the DCSs for the molecule of interest. ICSs can then be determined by integrating those DCSs, with the sum of the elastic and absorption ICSs (for all inelastic processes except rotations and vibrations) then giving the grand total cross sections (TCS). However, the AR does not take into account the molecular structure, so that it is really only applicable when the incident particles are so fast that they effectively "see" the target molecule as a sum of the individual atoms (typically above ~100 eV). To overcome this limitation, at least in part, the screening corrected AR (SCAR) method was introduced. This formalism accounts for the geometry of the molecule (atomic positions and bond lengths) by using some screening coefficients. With this correction, the range of validity was expected to be extended down to impact energies of ~30 eV for electron and positron scattering.

The IAM-SCAR approach described above does not account for vibrational and rotational excitations. However, for polar molecules such as H_2O, additional dipole-induced excitation cross sections can be calculated in the framework of the first Born approximation. These results can then be incorporated into our IAM-SCAR calculation in an incoherent way, just by adding up the cross sections as independent channels. The complete approach has been shown to be quite successful when applied to some polar molecules.[25] However, when the target molecule has a strong permanent dipole moment, as is the case for water, it is known that the FBA fails for medium and large scattering angles. In order to partially solve this problem we incorporated a correction which introduces a first-order corrective term to the differential cross sections for medium and large angles, but maintains the FBA for lower angles.[26]

We have used two forms of the optical potential in the present calculation – one which included the approximate treatment of positronium formation outlined above and one without. The inclusion of positronium formation in the optical potential has little effect on either the total elastic or

differential elastic cross sections, but has a significant effect, as will be seen, for the total inelastic cross section.

IV. RESULTS AND DISCUSSION

The total elastic and total inelastic cross sections are determined from the parallel energy loss spectrum measured with the RPA under conditions where a different magnetic field strength is applied at the RPA to that at the scattering cell, as has been described in some detail previously, e.g., Ref. 19. Briefly, the magnetic field at the RPA is reduced compared to the field at the scattering cell, and this effectively reduces the parallel energy spread which is introduced due to any angular scattering, allowing processes with different total energy loss to be separated,[19] as can also be seen from the positron transmission curve in Figure 1. The relative proportion of positrons undergoing elastic and inelastic collisions can then be measured, and hence the cross sections determined. It should be noted that due to current limitations in the practical application of the magnetic field ratio, combined with the energy resolution of the positron beam, rotational and vibrational excitation are not able to be distinguished from elastic scattering in the present case, so that the "quasi-elastic" cross sections presented here are, in fact, summed over these processes. As previously mentioned, the measured total inelastic cross section represents the sum of electronic and ionization processes but does not include positronium formation.

The total elastic and total inelastic cross sections are shown in Figures 2 and 3 respectively, and the tabulated cross section data are given in Tables II and III. In Figure 2 we

FIG. 3. Total inelastic cross section for positron scattering from water at energies up to 60 eV. The solid circles are the present cross section measurements and the long-dashed line is the distorted wave calculation of Hervieux *et al.*[25] for the direct ionization cross section. The solid black line is the IAM calculation for the total inelastic cross section with positronium modeled as discussed in the text, whilst the short dashed line is the IAM calculation without positronium.

also show the rotationally averaged, total elastic cross sections of Baluja *et al.*,[27] which have been calculated using the R-matrix formalism, and the present IAM calculation of the total elastic cross section. For the R-matrix calculation, the rotational averaging has been achieved using a Born-correction approach. This approach was also used in a more recent study by Zhang *et al.*[28] of positron (and electron) scattering from water molecules. In this work they applied a Born "top-up" approach to estimate forward scattering of positrons from water and to use the calculated differential cross sections to
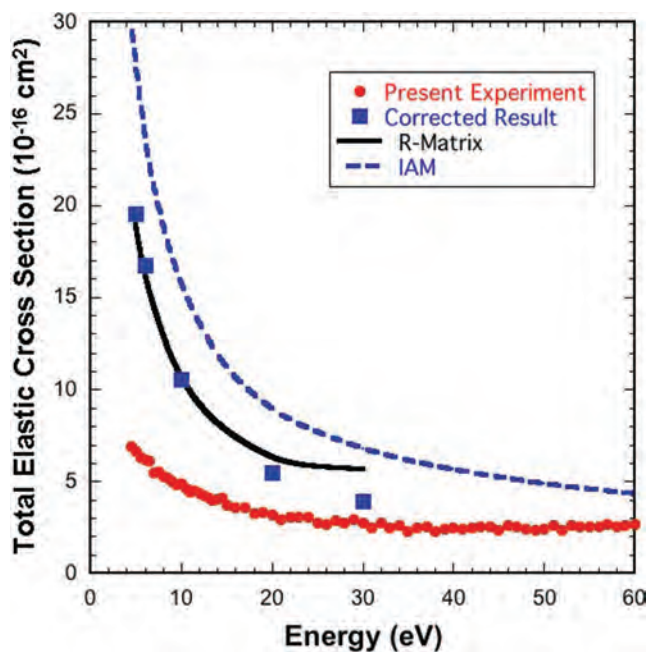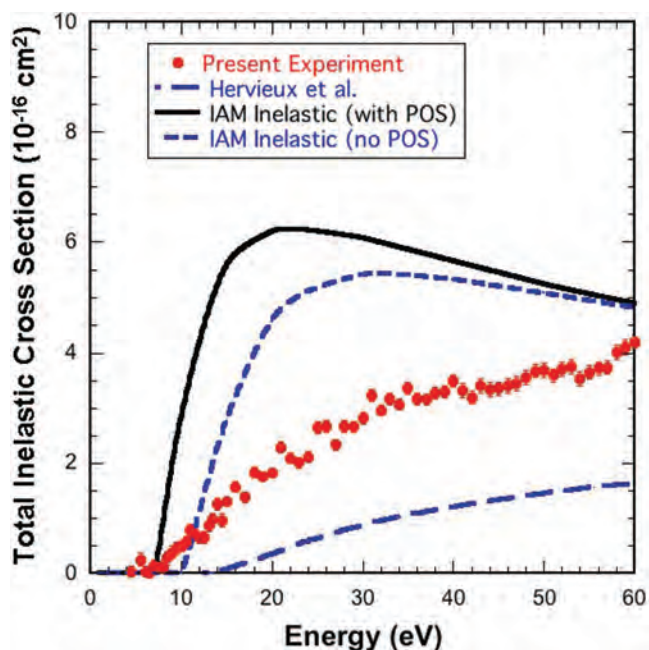

FIG. 2. Total elastic cross section for positron scattering from water at energies up to 60 eV. The dense array of solid circles are the raw cross section measurements, the filled squares are the cross section values after correcting for forward scattering, and the solid line is the R-matrix calculation (which was used for the correction calculation). The dashed line is the IAM calculation. The errors on the raw data points are roughly the size of the points themselves.

TABLE II. Absolute total elastic cross sections for positron scattering from water (units of 10^{-16} cm^2).

Energy (eV)	Cross section (10^{-16} cm^2)	Error	Corrected cross section
4.5	6.88	0.19	
5	6.64	0.18	19.53
5.5	6.34	0.18	
6	6.18	0.18	16.75
6.5	6.14	0.17	
7	5.50	0.17	
7.5	5.52	0.17	
8	5.30	0.17	
8.5	5.23	0.17	
9	5.03	0.16	
9.5	4.85	0.16	
10	4.86	0.13	10.53
10.5	4.64	0.16	
11	4.44	0.13	
11.5	4.52	0.16	

TABLE II. (*Continued.*)

Energy (eV)	Cross section (10^{-16} cm^2)	Error	Corrected cross section
12	4.35	0.13	
12.5	4.22	0.16	
13	4.12	0.13	
13.5	3.98	0.16	
14	4.03	0.13	
14.5	4.13	0.16	
15	3.69	0.11	
16	3.61	0.11	
17	3.57	0.11	
18	3.25	0.11	
19	3.30	0.11	
20	3.18	0.11	5.46
21	2.93	0.10	
22	3.09	0.10	
23	3.09	0.10	
24	3.05	0.11	
25	2.75	0.10	
26	2.64	0.10	
27	2.87	0.10	
28	2.75	0.10	
29	2.92	0.10	
30	2.75	0.10	3.91
31	2.51	0.10	
32	2.72	0.10	
33	2.46	0.10	
34	2.62	0.10	
35	2.30	0.10	
36	2.50	0.10	
37	2.53	0.10	
38	2.28	0.10	
39	2.39	0.10	
40	2.45	0.10	
41	2.39	0.11	
42	2.49	0.11	
43	2.53	0.11	
44	2.58	0.12	
45	2.38	0.11	
46	2.60	0.11	
47	2.52	0.12	
48	2.39	0.11	
49	2.34	0.12	
50	2.40	0.11	
51	2.63	0.12	
52	2.37	0.11	
53	2.61	0.12	
54	2.53	0.11	
55	2.56	0.12	
56	2.52	0.12	
57	2.70	0.12	
58	2.51	0.12	
59	2.64	0.11	
60	2.68	0.12	

correct previous total scattering measurements for forward scattering effects. This work was amongst the first to highlight the significant effect that forward scattering has on the body of measured, positron total cross sections for polar molecules.

In Figure 2 the raw total elastic measurements are indicated by the dense array of solid circles and they are seen

TABLE III. Absolute total inelastic cross section for positron scattering from water (units of 10^{-16} cm^2).

Energy (eV)	Cross section	Error
4.5	0.026	0.111
5	−0.063	0.111
5.5	0.251	0.114
6	0.015	0.109
6.5	0.005	0.109
7	0.122	0.110
7.5	0.111	0.112
8	0.121	0.112
8.5	0.273	0.113
9	0.380	0.116
9.5	0.460	0.113
10	0.481	0.098
10.5	0.560	0.114
11	0.782	0.101
11.5	0.719	0.122
12	0.644	0.100
12.5	0.657	0.114
13	0.862	0.101
13.5	0.974	0.121
14	1.27	0.110
14.5	0.967	0.125
15	1.30	0.091
16	1.57	0.095
17	1.38	0.091
18	1.83	0.096
19	1.76	0.094
20	1.83	0.095
21	2.28	0.098
22	2.09	0.097
23	2.01	0.096
24	2.11	0.095
25	2.64	0.104
26	2.67	0.104
27	2.34	0.098
28	2.67	0.104
29	2.66	0.102
30	2.82	0.102
31	3.24	0.108
32	2.96	0.104
33	3.17	0.107
34	3.07	0.106
35	3.36	0.107
36	3.17	0.107
37	3.16	0.104
38	3.28	0.106
39	3.31	0.109
40	3.50	0.109
41	3.33	0.126
42	3.20	0.122
43	3.41	0.125
44	3.34	0.122
45	3.36	0.126
46	3.41	0.123
47	3.45	0.125
48	3.56	0.127
49	3.67	0.125
50	3.68	0.128
51	3.59	0.127
52	3.71	0.125

TABLE III. (*Continued.*)

Energy (eV)	Cross section	Error
53	3.75	0.127
54	3.54	0.125
55	3.65	0.124
56	3.72	0.126
57	3.74	0.128
58	4.02	0.131
59	4.10	0.129
60	4.19	0.132

to lie well below both the R-matrix calculation (solid line) and the IAM cross section (dashed line). Note that the uncertainties on these experimental values are roughly the size of the data points (see Table I) and typically less than 5%. Baluja *et al.* also calculated differential elastic cross sections and these can be used, together with the known angular discrimination limits of the present apparatus (see Table I), to correct the raw, measured total elastic cross section for forward scattering effects. The corrected data are shown, at the

five discrete energies available from that theory, as the solid squares in Figure 2. The effect is clearly significant and results in a marked increase in the magnitude of the total elastic cross section, particularly at lower energies (e.g., about a factor of three at 5 eV). Accounting for the forward scattering also drastically improves the level of agreement between experiment and theory, with the corrected values being in excellent agreement with the R-Matrix calculation at energies up to 20 eV. The corrected values lie well below the IAM cross section, at all energies, by as much as a factor of two. At higher energies, where the corrections become small (or negligible), the measured cross section and the IAM values are beginning to merge. This is to be expected given the range of validity of the IAM-SCAR approach (E ∼ 30 eV and above) that has been discussed above.

Given the known sensitivity of positron scattering to polarization effects, and the difficulty, in general of reproducing these effects using close-coupling expansions of the type employed in the R-matrix approach, the level of agreement with the R-Matrix calculation is heartening. Water possesses both a significant dipole moment (∼1.85 D[29]) and dipole polarisability (∼10 a.u.) which, from our previous studies on polar
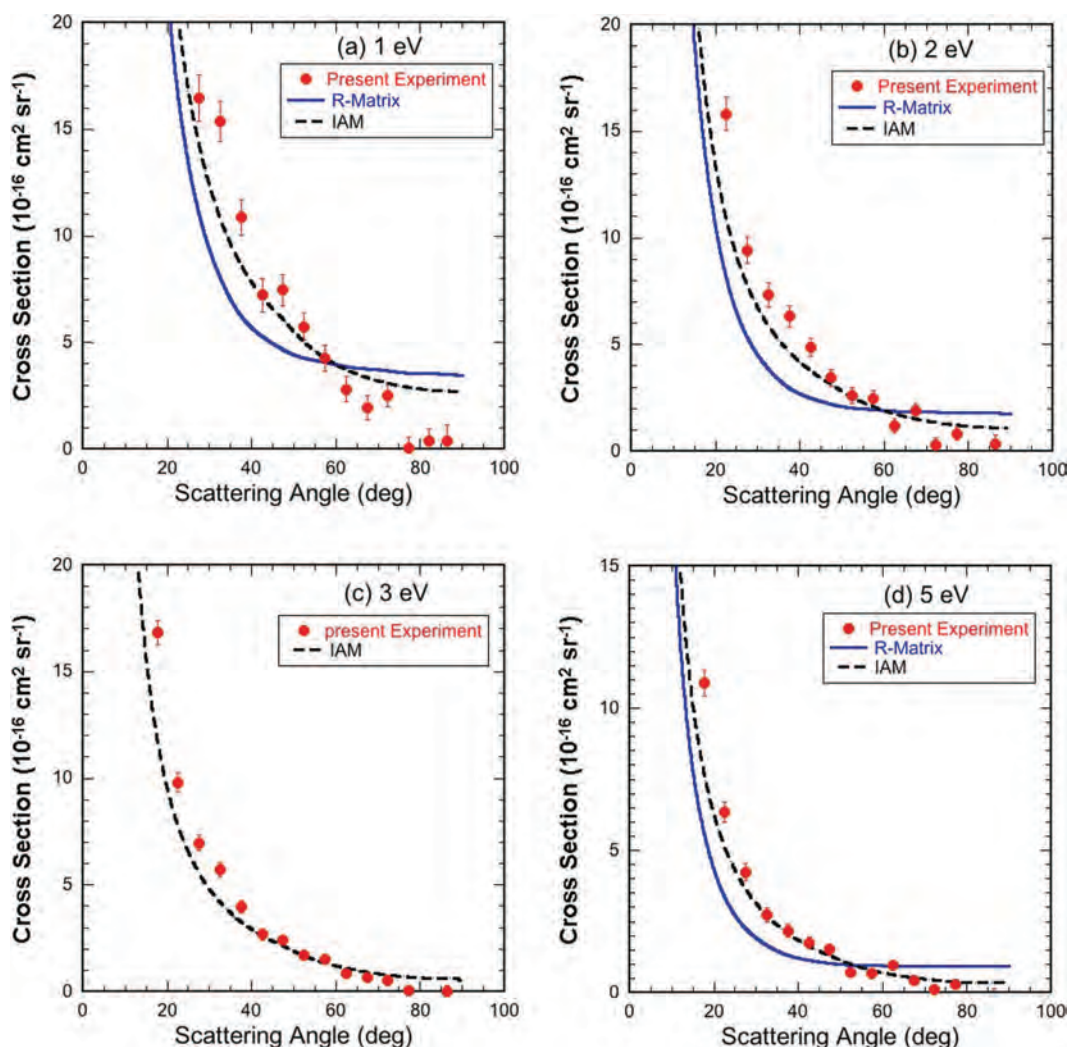

FIG. 4. Quasi-elastic differential cross sections for positron scattering from H_2O at energies of (a) 1 eV, (b) 2 eV, (c) 3 eV, and (d) 5 eV. The present experiment, R-matrix, and IAM calculations are noted on the plots.
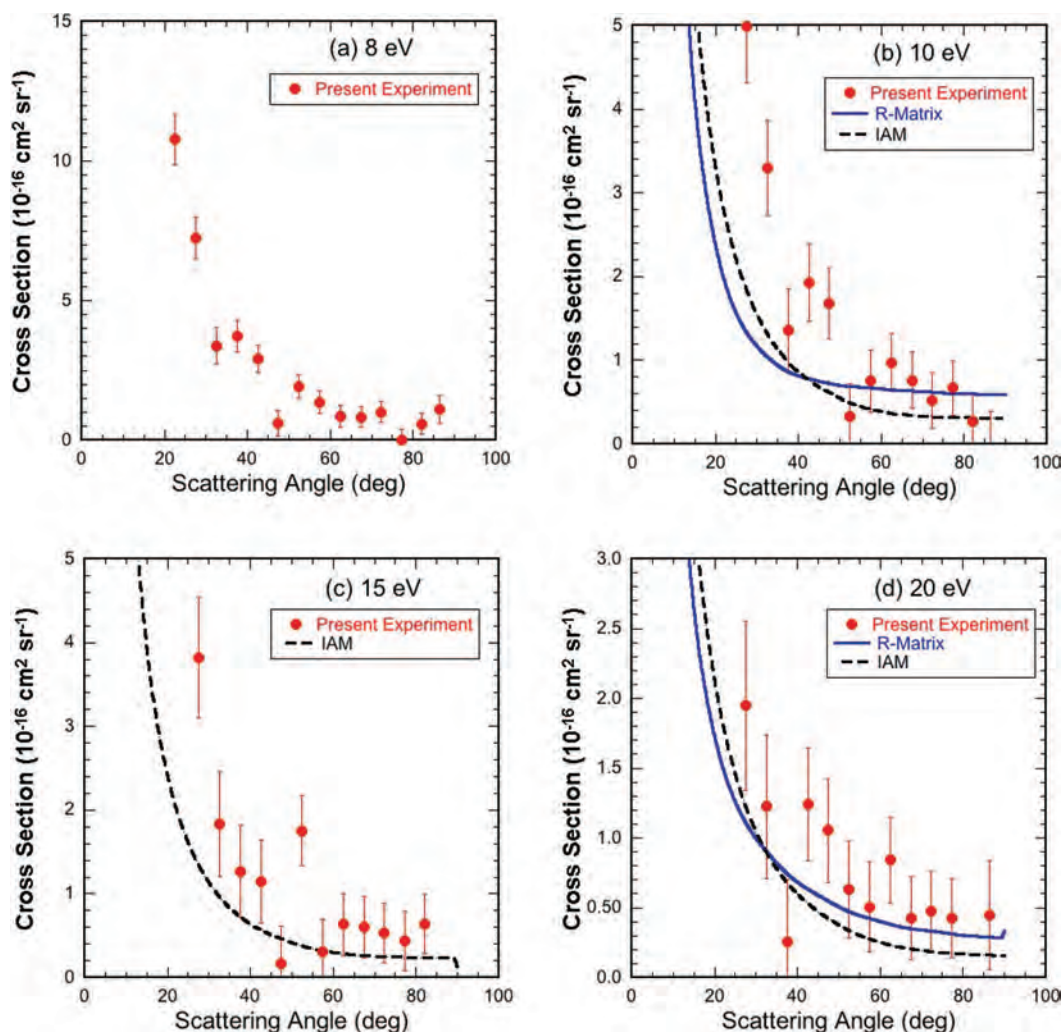
FIG. 5. Quasi-elastic differential cross sections for positron scattering from H_2O at energies of (a) 8 eV, (b) 10 eV, (c) 15 eV, and (d) 20 eV. The present experiment, R-matrix, and IAM calculations are noted on the plots.

species (e.g., Ref. 13), we would expect to have a significant effect on the scattering dynamics. The significant increase in the cross section as the energy decreases, in both experiment and theory, is indicative of the importance of these effects in the present case. Similar observations for positron scattering from other polar molecules have been made recently.[30, 31]

The measured total inelastic (excitation + ionization) cross section is shown in Figure 3, denoted as the solid circles, where it is compared with a continuum distorted wave calculation of the direct ionization cross section by Hervieux *et al.*,[32] and with the present theoretical estimates of the total inelastic cross section using the IAM approach. The measured total inelastic cross section rises slowly across the energy range measured from the $^1B_1$ electronic state threshold at $\sim$7.4 eV[33] to a maximum value of $\sim$ 4 Å^2 at 60 eV. As expected, this measured cross section is larger than the calculation of Hervieux *et al.*, which is for the ionization channel only. Although it was not possible, under the current experimental conditions, to fully resolve the contributions from electronic excitation and ionization to this cross section, the "energy loss" spectrum shown in Figure 1, at an energy of 45 eV, indicates that the majority of the measured total

inelastic cross section is due to ionization, as may intuitively be expected. As a consequence of this observation, it follows that the calculated direct ionization cross section[32] may underestimate the true magnitude at this energy.

The IAM calculation has been performed both with and without the inclusion (in a phenomenological fashion) of positronium formation in the optical potential. These two cross sections are also shown in Figure 3 and both variations predict a cross section which is larger than that observed, particularly in the near-threshold region. The calculation neglecting positronium appears to be in better agreement regarding the magnitude of the total inelastic cross section, while the energy dependence of both the IAM calculations differs significantly from experiment. Both calculations begin to merge at higher energies, which is to be expected, and are closer in magnitude to the experiment. Tabulated values of the present measured total inelastic cross section can be found in Table III.

The differential, quasi-elastic scattering cross sections are shown in Figures 4 and 5, and listed in Table IV, at energies between 1 and 20 eV. Also shown in several of these figures are the R-matrix DCS calculations

TABLE IV. Elastic differential cross sections for positron scattering from water (units of 10^{-16} cm^2 sr^{-1}).

Angle	1 eV		2 eV		3 eV	
	DCS	Error	DCS	Error	DCS	Error
13	…	…	…	…	45.19	0.79
18	…	…	25.61	0.98	16.83	0.57
23	25.71	1.32	15.82	0.78	9.81	0.45
28	16.45	1.09	9.43	0.65	6.97	0.37
33	15.36	0.94	7.33	0.56	5.72	0.32
38	10.86	0.84	6.32	0.49	3.97	0.28
43	7.22	0.77	4.87	0.45	2.68	0.26
47	7.46	0.72	3.44	0.41	2.42	0.24
52	5.74	0.65	2.62	0.38	1.71	0.22
57	4.26	0.62	2.47	0.37	1.53	0.21
62	2.80	0.59	1.17	0.34	0.87	0.20
67	1.93	0.56	1.91	0.33	0.68	0.19
72	2.51	0.53	0.30	0.32	0.51	0.19
77	0.03	0.55	0.83	0.32	0.07	0.18
82	0.39	0.56	− 0.47	0.33	− 0.12	0.19
86	0.40	0.74	0.31	0.43	0.02	0.25
	5 eV		8 eV		10 eV	
13	21.56	0.64	…	…	…	…
18	10.88	0.46	25.89	1.17	18.53	1.00
23	6.35	0.36	10.77	0.90	8.76	0.81
28	4.23	0.30	7.24	0.75	4.99	0.67
33	2.73	0.26	3.38	0.65	3.30	0.57
38	2.18	0.24	3.72	0.57	1.36	0.50
43	1.76	0.21	2.91	0.51	1.93	0.46
47	1.52	0.20	0.59	0.47	1.68	0.43
52	0.70	0.18	1.91	0.43	0.33	0.40
57	0.67	0.17	1.36	0.40	0.75	0.37
62	0.96	0.16	0.85	0.40	0.97	0.35
67	0.41	0.15	0.83	0.38	0.76	0.34
72	0.12	0.15	1.01	0.37	0.52	0.33
77	0.30	0.15	0.02	0.37	0.67	0.33
82	− 0.11	0.15	0.58	0.37	0.27	0.33
86	− 0.07	0.20	1.09	0.50	− 0.05	0.43
	15 eV		20 eV		25 eV	
13	36.67	1.51	…	…	…	…
18	10.70	1.11	…	…	…	…
23	6.09	0.86	…	…	2.66	0.58
28	3.82	0.72	1.95	0.61	3.46	0.49
33	1.84	0.63	1.22	0.51	0.74	0.42
38	1.27	0.55	0.25	0.45	0.38	0.37
43	1.15	0.50	1.24	0.40	0.55	0.33
47	0.17	0.45	1.05	0.37	0.90	0.31
52	1.76	0.42	0.63	0.35	0.25	0.28
57	0.31	0.39	0.50	0.32	0.90	0.27
62	0.63	0.37	0.84	0.31	0.21	0.25
67	0.60	0.37	0.43	0.30	1.09	0.24
72	0.53	0.35	0.48	0.29	0.07	0.24
77	0.44	0.35	0.43	0.28	0.37	0.24
82	0.64	0.35	− 0.36	0.29	0.12	0.24
86	…	…	0.45	0.39	0.03	0.32

of Baluja *et al.*, and the present IAM calculations, both of which include rotations, as does the experimental cross section. In all cases where we illustrate the IAM calculations, we have used the approach which included positronium formation. With the possible exception of 20 eV,

where the two IAM approaches varied by at most a few percent across the angular range, there is no significant difference between these two approaches for the elastic DCS at the energies and angles we are considering.

The lowest energy measurement is at 1 eV (Figure 4(a)) where we compare with both the R-matrix calculation and the IAM cross section. Interestingly, at this energy (and at all subsequent energies where such comparison is possible) the experimental cross section is larger than the R-matrix result at most scattering angles. Given the comparison of the total elastic cross section in Figure 2, where this theory and (corrected) experiment where in good agreement, one could conclude that the theoretical DCS must be significantly larger at small scattering angles. The significant surprise at this energy is the excellent level of agreement between the experiment and the IAM calculation – something quite unexpected given that this theory has not indicated such agreement with experiment (at the total cross section level for either electrons or positrons) at energies below about 30 eV in previous applications. At energies of 1, 3, and 5 eV (Figures 4(a)–4(c), respectively) the experimental DCS decreases gradually with increasing angle, and without any prominent features, from relatively high magnitude at the smallest measured angle, to close to zero at the largest. The cross section at small angles also decreases rapidly with energy over this range, an observation which is typical of a strong dipole scattering system. Once again, at 3 and 5 eV, we see good agreement in general with the R-Matrix calculation and excellent agreement with the IAM cross section – again something that is quite unexpected.

At energies above 5 eV, the measurements were taken with a reduced magnetic field in the RPA section (5 times smaller than scattering cell region) in order to separate out contributions from inelastic electronic excitation. At energies of 8, 10, 15, and 20 eV (Figures 5(a)–5(d), respectively) we see the same overall behavior of the cross section and an overall reduction in magnitude with increasing energy. Comparison with the R-matrix and IAM calculations at 5 eV shows a reasonably good level of agreement in magnitude and angular dependence with both, with the IAM calculation passing through the experimental points at most angles. The agreement between experiment and theory is worse at 10 eV (except for the large angle measurements) while at 15 and 20 eV both calculations are generally lower in magnitude than the experimental values.

V. CONCLUSIONS

We have presented new experimental data, and IAM calculations, for elastic and inelastic scattering of positrons from water vapour, at energies spanning the range between 1 and 60 eV, including the first measurements of both total and differential elastic scattering, and total inelastic scattering. The agreement between experiment and theory for the total elastic cross section is acceptable, particularly with the R-Matrix calculation when the effects of forward angle differential scattering, which are appreciable, are taken into account. For the total inelastic cross section, the comparison with the direct ionization cross section of Hervieux *et al.* is

largely consistent with expectations, while the experiment is generally lower in magnitude than both forms of the IAM calculation for this cross section. The results for these two measurements indicate that between 20 and 60 eV, the magnitude of the total elastic and total inelastic (not including Ps production) cross sections are roughly equivalent.

At the differential elastic scattering level the results were somewhat surprising. The R-matrix calculation of Baluja *et al.* shows generally good agreement with experiment across the energy and angular range, with perhaps the best agreement being at 20 eV. The unexpected result, from our perspective, was the excellent level of agreement between the IAM calculations of differential elastic scattering and the present experiment. Most previous applications of this semi-phenomenological approach have returned the expected outcome that it begins to break down for projectile energies below about 30 eV. This has been the case particularly for electron applications to both small and large molecules. However, a recent application of the technique to positron scattering from the pyrimidine molecule[34] indicated a similar level of agreement between experiment and theory for the DCS as we see here for water. So the excellent agreement that is shown at lower energies in the present comparison is puzzling and, while it may prove to be fortuitous, it is not a lone example for positron interactions with molecules. One other aspect that is worth noting in the comparison with the IAM calculation is that while there is very good agreement at the DCS level (for those angles where we can compare) the present total elastic cross section lies well below the IAM at all energies, particularly low energies. This is no doubt due to the significant contribution that comes to the total cross section from the forward angles not measured in the present experiment.

Nonetheless, the agreement with this theory, and with the R-matrix calculation, is consistently good for the processes studied and that gives us confidence that both theoretical approaches could be used with some confidence to provide the extensive data sets that are required for positron transport and modeling purposes.

ACKNOWLEDGMENTS

[1]L. D. Barnes, S. J. Gilbert, and C. Surko, Phys. Rev. A **67**, 032706 (2003).

[2]L. D. Barnes, J. A. Young, and C. Surko, Phys. Rev. A **74**, 012706 (2006).

[3]A. C. L. Jones, C. Makochekanwa, P. Caradonna, D. S. Slaughter, J. R. Machacek, R. P. McEachran, J. P. Sullivan, S. J. Buckman, A. D. Stauffer, I. Bray, and D. V. Fursa, Phys. Rev. A **83**, 032701 (2011).

[4]P. Caradonna, J. P. Sullivan, A. Jones, C. Makochekanwa, D. Slaughter, D. W. Mueller, and S. J. Buckman, Phys. Rev. A **80**, 060701(R) (2009).

[5]P. Caradonna, A. Jones, C. Makochekanwa, D. S. Slaughter, J. P. Sullivan, S. J. Buckman, I. Bray, and D. V. Fursa, Phys. Rev. A **80**, 032710 (2009).

[6]J. R. Machacek, C. Makochekanwa, A. Jones, P. Caradonna, D. Slaughter, R. P. McEachran, J. P. Sullivan, S. J. Buckman, S. Bellm, B. Lohmann, D. Fursa, I. Bray, D. W. Mueller, and A. D. Stauffer, New J. Phys. **13**, 125004 (2011).

[7]D. B. Cassidy, T. H. Hisakado, H. W. K. Tom, and A. P. Mills, Jr., Phys. Rev. Lett. **109**, 073401 (2012).

[8]G. F. Gribakin and C. M. R. Lee, Phys. Rev. Lett. **97**, 193201 (2006).

[9]R. Utamuratov, A. S. Kadyrov, D. V. Fursa, and I. Bray, J. Phys. B: At. Mol. Opt. Phys. **43**, 031001 (2010).

[10]R. D. White, J. P. Sullivan, A. Bankovic, S. Dujko, R. E. Robson, Z. Lj. Petrovic, G. Garcia, M. J. Brunger, and S. J. Buckman, *Radiation Damage in Biomolecular Systems*, edited by M. Fuss and G. García (Springer, 2012).

[11]A. G. Sanz, M. C. Fuss, A. M. Roldan, F. Blanco, P. Limao-Vieira, M. J. Brunger, S. J. Buckman, and G. Garcia, Int. J. Radiat. Biol. **88**, 71–76 (2012).

[12]D. Bailey, W. Townsend, P. Valk, and M. Maisey, *Positron Emission Tomography* (Springer-Verlag, London, 2005).

[13]C. Makochekanwa, A. Bankovic, W. Tattersall, A. Jones, P. Caradonna, D. Slaughter, J. P. Sullivan, K. Nixon, M. J. Brunger, Z. Lj. Petrovic, and S. J. Buckman, New J. Phys. **11**, 103036 (2009).

[14]S. Uehara and H. Nikjoo, Radiat. Environ. Biophys. **35**, 153 (1996).

[15]B. Boudaiffa, P. Cloutier, D. Hunting, M. A. Huels, and L. Sanche, Science **287**, 1658 (2000).

[16]F. Martin, P. D. Burrow, Z. Cai, P. Cloutier, D. Hunting, and L. Sanche, Phys. Rev. Lett. **93**, 068101 (2004).

[17]J. P. Sullivan, A. Jones, P. Caradonna, C. Makochekanwa, and S. J. Buckman, Rev. Sci. Instrum. **79**, 113105 (2008).

[18]C. Makochekanwa, J. Machacek, A. Jones, P. Caradonna, D. S. Slaughter, R. P. McEachran, J. P. Sullivan, S. J. Buckman, S. Bellm, B. Lohmann, D. W. Mueller, A. D. Stauffer, D. Fursa, I. Bray, and M. Hoshino, Phys. Rev. A **83**, 032721 (2011).

[19]J. P. Sullivan, S. J. Gilbert, J. P. Marler, R. G. Greaves, S. J. Buckman, and C. M. Surko, Phys. Rev. A **66**, 042708 (2002).

[20]J. P. Sullivan, C. Makochekanwa, A. Jones, P. Caradonna, D. S. Slaughter, J. Machacek, R. P. McEachran, D. W. Mueller, and S. J. Buckman, J. Phys. B: At. Mol. Opt. Phys. **44**, 035201 (2011).

[21]F. Blanco and G. Garcia, J. Phys. B: At. Mol. Opt. Phys. **42**, 145203 (2009).

[22]L. Chiari, A. Zecca, S. Girardi, E. Trainotti, G. Garcıa, F. Blanco, R. P. McEachran, and M. J. Brunger, J. Phys. B: At. Mol. Opt. Phys. **45**, 215206 (2012).

[23]L. Chiari, E. Anderson, W. Tattersall, J. R. Machacek, P. Palihawadana, C. Makochekanwa, J. P. Sullivan, G. Garcia, F. Blanco, R. P. McEachran, M. J. Brunger, and S. J. Buckman, J. Chem. Phys. **138**, 074301 (2013).

[24]R. P. McEachran, D. L. Morgan, A. G. Ryman, and A. D. Stauffer, J. Phys. B: At. Mol. Phys. **10**, 663 (1977).

[25]L. Chiari, A. Zecca, G. Garcıa, F. Blanco, and M. J. Brunger, J. Phys. B: At. Mol. Opt. Phys. **46**, 235202 (2013).

[26]A. G. Sanz, M. C. Fuss, F. Blanco, Z. Mašín, J. D. Gorfinkiel, R. P. McEachran, M. J. Brunger, and G. García, Phys. Rev. A **88**, 062704 (2013).

[27]K. L. Baluja, R. Zhang, J. Franz, and J. Tennyson, J. Phys. B: At. Mol. Opt. Phys. **40**, 3515 (2007).

[28]R. Zhang, A. Faure, and J. Tennyson, Phys. Scr. **80**, 015301 (2009).

[29]S. J. Suresh and V. M. Naik, J. Chem. Phys. **113**, 9727 (2000).

[30]A. Zecca, L. Chiari, G. Garcia, F. Blanco, E. Trainotti, and M. J. Brunger, J. Phys. B: At. Mol. Opt. Phys. **43**, 215204 (2010).

[31]A. Zecca, L. Chiari, A. Sarkar, and M. J. Brunger, J. Phys. B: At. Mol. Opt. Phys. **41**, 085201 (2008).

[32]P.-A. Hervieux, O. A. Fojon, C. Champion, R. D. Rivarola, and J. Hanssen, J. Phys. B: At. Mol. Opt. Phys. **39**, 409 (2006).

[33]P. A. Thorn, M. J. Brunger, P. J. O. Teubner, N. Diakomichalis, T. Maddern, M. A. Bolorizadeh, W. R. Newell, H. Kato, M. Hoshino, H. Tanaka, H. Cho, and Y.-K. Kim, J. Chem. Phys. **126**, 064306 (2007).

[34]P. Palihawadana, R. Boadle, L. Chiari, E. K. Anderson, J. R. Machacek, M. J. Brunger, S. J. Buckman, and J. P. Sullivan, Phys. Rev. A **88**, 012717 (2013).